# RESONANCE COMPENSATION STUDIES AT THE FNAL RECYCLER RING

By

Cristhian Gonzalez-Ortiz

A DISSERTATION

Submitted to
Michigan State University
in partial fulfillment of the requirements
for the degree of

Physics—Doctor of Philosophy

2024

# ABSTRACT

## ACKNOWLEDGEMENTS

Your acknowledgements here.

## TABLE OF CONTENTS

## LIST OF ABBREVIATIONS

**MSU** Michigan State University

**FNAL** Fermilab National Accelerator Laboratory

**RR** Recycler Ring

**MI** Main Injector

**RDTs** Resonance Driving Terms

**NuMI** Neutrinos at the Main Injector

**PSB** CERN Proton Synchrotron Booster

# CHAPTER 1

# INTRODUCTION

The following thesis will explore the compensation of third-order resonances in the Fermilab Recycler Ring. This first chapter introduces the motivation behind this thesis work. The second chapter summarizes single particle dynamics with the help of exponential Lie operators and moves forward to introduce a relevant concept of collective beam dynamics: the space charge tune shift. This theoretical overview gives segue into the third chapter of this thesis, where the Recycler Ring is introduced and described in detail. Motivation for the compensation of third order resonances is given in this chapter under the framework of current and future operation of the RR. With the basic physics concepts and the description of the machine put in place, the fourth chapter describes in full detail the scheme and experiments developed in order to compensate third order resonances at low intensities. Before moving to explore the Recycler Ring at high intensities, chapter five provides an interlude in order to show a series of experiments done at the CERN PS Booster. These experiments explore the use of advanced optimization algorithms in the aid of compensating multiple resonance lines simultaneously. Coming back to Fermilab, chapter six showcases the studies and experiments done at high intensities in the RR in order to understand the interplay between the compensation of resonance lines and space charge effects. Finally, chapter seven brings down the curtain by providing some general conclusions and future work stemming from this thesis. For now, let this first chapter introduce some relevant concepts.

# CHAPTER 2

# BEAM DYNAMICS IN RINGS

## 2.1 Lie Maps in Accelerator Physics

The most basic element of a particle accelerator can be thought of as a black box. This black box takes some single charged particle with initial transverse coordinates $\left(x_0, x_0', y_0, y_0'\right)$, as defined in a Frenet-Serret coordinate system, and maps them to some final coordinates $\left(x_f, x_f', y_f, y_f'\right)$. For simplicity, any longitudinal effect will not be taken into account for this analysis, but can be easily incorporated. By gathering the initial coordinates into a vector, i.e. $\vec{X}_0 = \left(x_0, x_0', y_0, y_0'\right)$, and doing the same for the final coordinates, i.e., $\vec{X}_f = \left(x_f, x_f', y_f, y_f'\right)$, one can define the mapping $\mathcal{M}$ that relates both vectors, such that:

$$\vec{X}_f = \mathcal{M}\vec{X}_0. \tag{2.1}$$

For a charged particle inside some accelerator element that can be described using Hamiltonian dynamics, the mapping $\mathcal{M}$ can be understood in terms of Poisson brackets and exponential Lie operators [1–4].

Let $\vec{X} = (q_1, p_1, \ldots, q_n, p_n)$ be a 2n dimensional vector, made from $n$ pairs of canonical coordinates $(q_i, p_i)$ that make up the $2n$ dimensional phase space. And let two arbitrary functions $f\left(\vec{X}; s\right)$ and $g\left(\vec{X}; s\right)$ be functions of $\vec{X}$ and $s$, where $s$ plays the role of the independent "time" coordinate. The Poisson brackets $[\bullet, \bullet]$ can be defined as:

$$[f, g] = \sum_{i=1}^{n} \frac{\partial f}{\partial q_i}\frac{\partial g}{\partial p_i} - \frac{\partial f}{\partial p_i}\frac{\partial g}{\partial q_i}. \tag{2.2}$$

Using this definition, one can explicitly write out the Poisson bracket definition for a 4 dimensional phase space described by state vector $\vec{X} = (x, x', y, y')$. This reads:

$$[f, g] = \frac{\partial f}{\partial x}\frac{\partial g}{\partial x'} - \frac{\partial f}{\partial x'}\frac{\partial g}{\partial x} + \frac{\partial f}{\partial y}\frac{\partial g}{\partial y'} - \frac{\partial f}{\partial y'}\frac{\partial g}{\partial y}. \tag{2.3}$$

The Lie operator $: f :$ acts on some function $g$ and is the adjoint operator of the Poisson bracket operator. Its definition reads:

$$: f : g = [f, g]\,. \tag{2.4}$$

This specific $: \bullet :$ notation allows for a compact notation in order to define the exponential Lie operator. The exponential Lie operator of an arbitrary function $f$ is defined as

$$e^{:f:}\bullet = \sum_{k=0}^{\infty} \frac{1}{k!} (: f :)^k \bullet . \tag{2.5}$$

It turns out that for a Hamiltonian system, the mapping of coordinates from $\vec{X}_0$ to $\vec{X}_f$ follows the expression:

$$\vec{X}_f = e^{-\ell:H:}\vec{X}\Big|_{\vec{X}=\vec{X}_0}, \tag{2.6}$$

which is known as a Lie Map [2]. In this case, $\ell$ corresponds to the integration length of the independent coordinate. For example, for a particle traversing a magnet which has length $L$, the integration length is $\ell = L$. When looking at the one-turn map, the integration length corresponds to the circumference $C$ of the accelerator over an effective Hamiltonian $H_{eff}$. Furthermore, if working with action-angle variables, the integration length $\ell$ would just be the phase advance $\mu$.

### 2.2 One-turn Map and Normal Form

The one-turn map $\mathcal{M}_1$ of a circular accelerator is the composition ($\circ$) of mappings from every element in the ring. Choosing an arbitrary initial point at $s = 0$ and going around the ring, the one-turn map describes the transformation of coordinates after one turn, i.e., $\vec{X}_{N=1} = \mathcal{M}_1\vec{X}_0$. This map composition reads:

$$\mathcal{M}_1 = M_{N+1} \circ e^{:h_N:} \circ \cdots \circ e^{:h_2:} \circ M_2 \circ e^{:h_1:} \circ M_1 = M_{N+1}e^{:h_N:} \ldots e^{:h_2:}M_2e^{:h_1:}M_1, \tag{2.7}$$

where $M_i$ is the matrix representation of a linear mapping, that does not couple $x - y$ plane, e.g., drift space mapping, quadrupole mapping. On the other hand, the map $e^{:h_i:}$ represents any linear or non-linear mapping that can be found around the machine and can be considered a perturbation to the ideal lattice including coupling elements, e.g., skew quadrupoles, higher order multipole elements. Figure 2.1 illustrates the procedure to build the one-turn map for a circular accelerator.

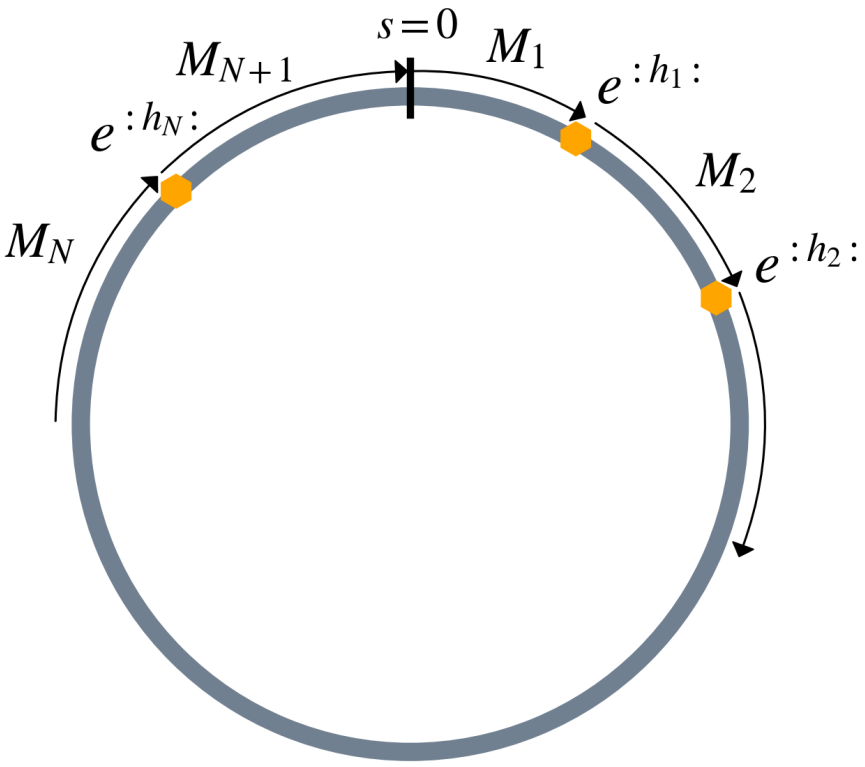


Figure 2.1 Diagram of an arbitrary circular accelerator in order to illustrate the one-turn map.

Through the use of the Baker-Campbell-Hausdorff formula , Eq. 2.7 can be collapsed to the expression

$$\mathcal{M}_1 = e^{-C:H_{eff}:}, \tag{2.8}$$

where $C$ is the circumference of the ring and $H_{eff}$ is the effective Hamiltonian of the machine over one turn. As mentioned earlier, for most cases, it is of interest to look at the perturbations to the linear uncoupled dynamics of the design lattice. With this in mind, Eq. 2.8 can be rewritten as:

$$\mathcal{M}_1 = e^{:h:}R, \tag{2.9}$$

where $R$ is a rotation matrix encoding the linear uncoupled dynamics of the ideal lattice. On the other hand, the term $e^{:h:}$ encodes the perturbations to this ideal situation. It is worth pointing out that for the case $h = 0$, the traditional Courant-Snyder variables are recovered.

The Courant-Snyder variables $(\hat{x},\hat{p}_x,\hat{y},\hat{p}_y)$ or normalized phase space coordinates can be written for a linear uncoupled case as:

$$\hat{u} = \sqrt{2J_u}\cos\left(\phi_u + \phi_{u_0}\right); \tag{2.10}$$

$$\hat{p}_u = -\sqrt{2J_u}\sin\left(\phi_u + \phi_{u_0}\right), \tag{2.11}$$

where $u$ can stand either for the $x$ or $y$ coordinate, $J_u$ and $\phi_u$ correspond to the action-angle variables and $\phi_{u_0}$ corresponds to the initial phase. For the case where perturbations exist, i.e., $h \neq 0$, the action $J_u$ is not constant anymore and will be a function of $\phi_u$.

The Normal Form formalism is introduced at this point in order to find amplitude-independent coordinates $I_u$ and $\psi_u$, such that the motion just depends on $\psi_u$ at a constant $I_u$, with some initial phase $\psi_{u_0}$. These are known as non-linear action-angle variables. The variables $I_u$ and $\psi_u$ are calculated from the transformation $e^{-:F:}$ acting on $J_u$ and $\phi_u$. Without loss of generality, the generating function $F$ can be written as a Fourier expansion over the objective space $(I_x, \psi_x, I_y, \psi_y)$ such that:

$$F = \sum_{jklm} f_{jklm}\left(2I_x\right)^{\frac{j+k}{2}}\left(2I_y\right)^{\frac{l+m}{2}} e^{i\left[(j-k)(\psi_x+\psi_{x0})+(l-m)\left(\psi_y+\psi_{y0}\right)\right]}. \tag{2.12}$$

In a similar fashion, the argument of the Lie operator $e^{:h:}$ from Eq. 2.9 can be expanded as:

$$h = \sum_{jklm} h_{jklm}\left(2J_x\right)^{\frac{j+k}{2}}\left(2J_y\right)^{\frac{l+m}{2}} e^{i\left[(j-k)(\phi_x+\phi_{x0})+(l-m)\left(\phi_y+\phi_{y0}\right)\right]}. \tag{2.13}$$

For Eqs. 2.12 and 2.13, the integer indices $j, k, l, m$ run from 0 to infinity, and correspond to the four degrees of freedom for transverse phase space.

The terms $f_{jklm}$ are known as generating function coefficients. The terms $h_{jklm}$ are known as Hamiltonian coefficients or resonance driving terms (RDTs). Section 2.4 will take a closer look into how RDTs can be used to characterize the non-linear dynamics of accelerators. The generating function coefficients $f_{jklm}$ can be related to the Hamiltonian resonance driving terms $h_{jklm}$ through the following relation[3, 5]:

$$f_{jklm} = \frac{h_{jklm}}{1 - e^{2\pi i\left[(j-k)Q_x+(l-m)Q_y\right]}}. \tag{2.14}$$

## 2.3 Resonances in Circular Accelerators

[6]

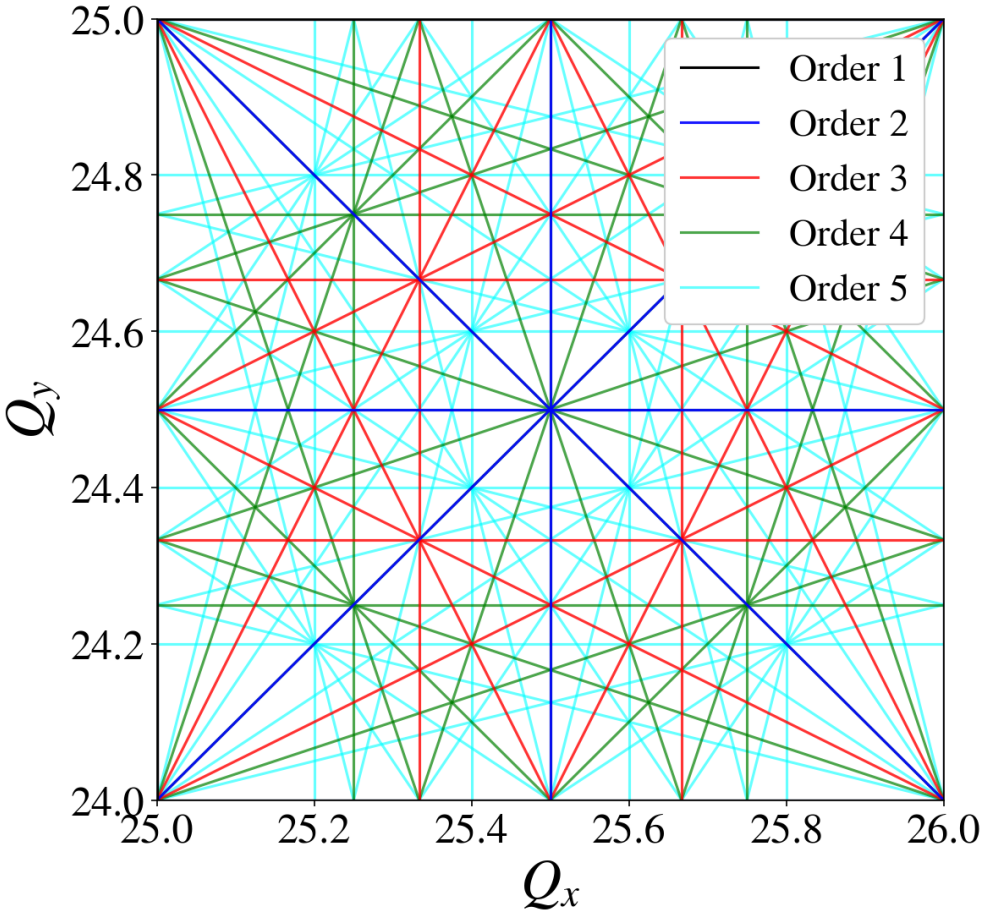


Figure 2.2 Tune diagram with resonance lines up to fifth order, enclosing the operation point of the Recycler Ring.

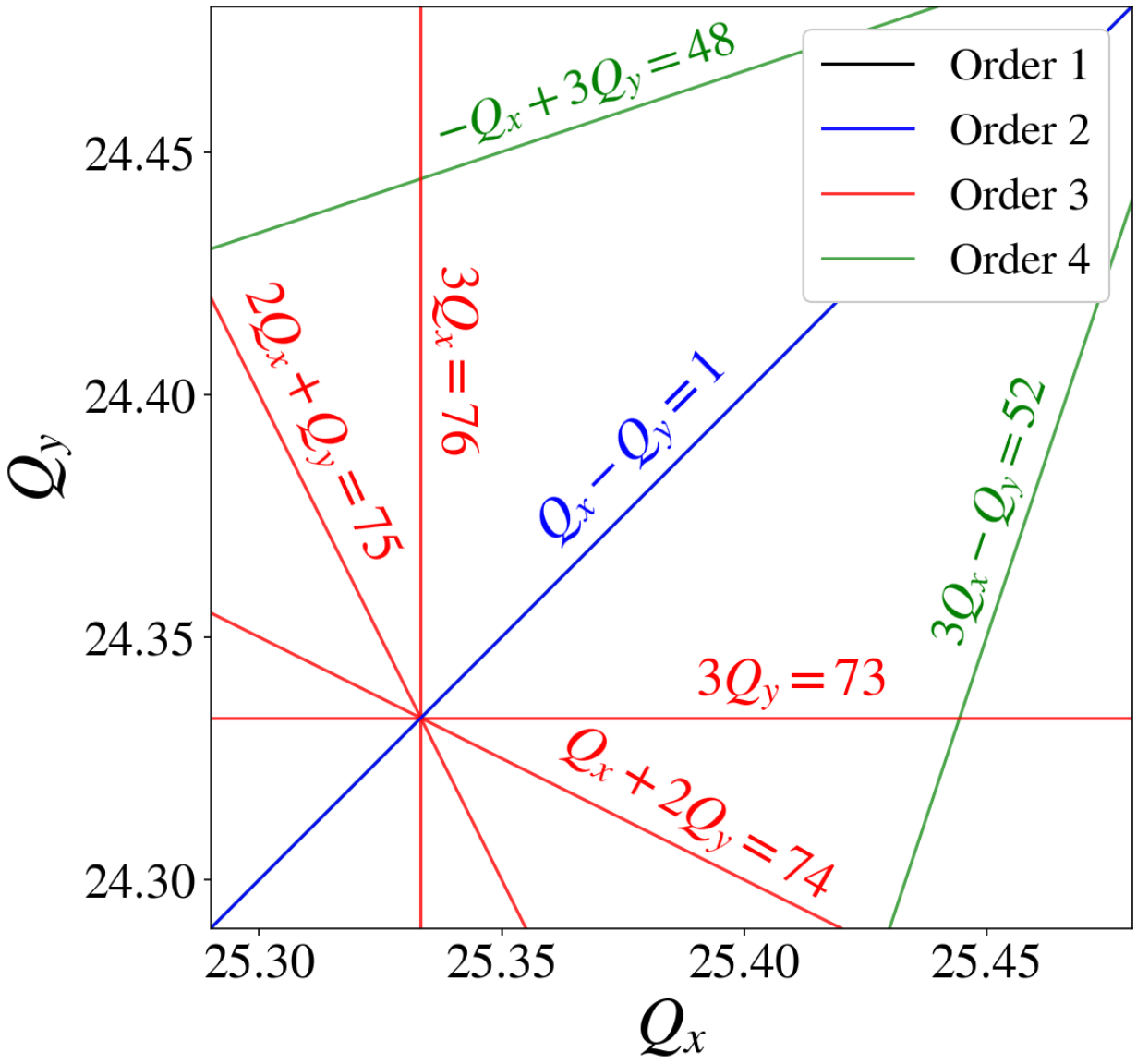


Figure 2.3 Portion of the tune diagram enclosing the operational tunes of the Recycler Ring.

### 2.4 Resonance Driving Terms

The resonance basis can be built by getting the quantity $h_u^{\pm} = \hat{u} \pm \hat{p_u}$ in terms of the number of turns $N$ . Specifically, for $h_x^-$ this reads:

$$h_x^-(N) = \sqrt{2I_x} e^{i\left(2\pi Q_x N + \psi_{x_0}\right)} - 2i \sum_{jklm} j f_{jklm} \left(2I_x\right)^{\frac{j+k-1}{2}} \left(2I_y\right)^{\frac{l+m}{2}} e^{i\left[(1-j+k)\left(2\pi Q_x N + \psi_{x_0}\right) + (m-l)\left(2\pi Q_y N + \psi_{y_0}\right)\right]}, \quad (2.15)$$

where $Q_x$ and $Q_y$ are the horizontal and vertical tune [3].

In general, RDTs are defined by the order in which they enter the one-turn normal form Hamiltonian [5]. The general expression to define RDTs reads:

$$h_{jklm} = \Xi_{jklm} \sum_i L_i \beta_{xi}^{\frac{j+k}{2}} \beta_{yi}^{\frac{l+m}{2}} V_{ni} e^{i\left[(j-k)\phi_{xi}+(l-m)\phi_{yi}\right]}, \tag{2.16}$$

where $\Xi_{jklm}$ is just a constant defined as:

$$\Xi_{jklm} = -\frac{q}{p_0}\frac{1}{2^n}\frac{1}{n}\binom{n}{l+m}\binom{j+k}{j}\binom{l+m}{l}. \tag{2.17}$$

For Eqs. 2.16 and 2.17, $n = j + k + l + m$ represents the order of the resonance. The sum over $i$ is done over all multipoles of order $n$ and length $L_i$ that either have a normal component $V_{ni} = B_{ni}$ if $l + m$ is even, or a skew component $V_{ni} = A_{ni}$ if $l + m$ is odd. The symbols for $\beta_{xi}$, $\beta_{yi}$, $\phi_{xi}$ and $\phi_{yi}$ represent the beta functions and phase advances in each plane, respectively.

### 2.5 Space Charge Tune Shift

# CHAPTER 3

## THE FNAL RECYCLER RING

The Fermilab Recycler Ring (RR) is one of the circular accelerators located in the Fermilab Accelerator Complex. It was originally designed to store and accumulate antiprotons that remained from a Tevatron event [7]. The recycling of antiprotons was deemed ineffective and was never operationally implemented [8]. Since 2011, the RR has been repurposed to act as a pre-injector to the Main Injector (MI) by storing and accumulating protons [9]. It is worth pointing out, that the MI and the RR share the same tunnel, which has a circumference of 3.319 km (2.062 mi).

The MI/RR complex is fed protons by the Proton Source, which by itself consists of the Pre-Accelerator, the Linear Accelerator (Linac), and the Booster. The Pre-Accelerator systems provide $H^-$ ions to the Linac, where they are accelerated to an energy of 400 MeV. After this, the beam is injected into the Booster, which is a rapid-cycling synchrotron operating at a 15 Hz repetition rate. During this injection process, the $H^-$ beam passes through a carbon stripping foil, and it incorporates to the circulating proton beam. The Booster ramps the energy up from 400 MeV to 8 GeV. This 8 GeV proton beam can either go to the Booster Neutrino Experiments or get injected into the Recycler Ring. Once in RR the beam has two possible destinations: 1) high energy neutrino experiments through MI or 2) Muon Campus. For the latter, proton beam gets rebunched from 53 MHz to 2.5 MHz and transported to Muon Campus. For high energy neutrino experiments, the proton beam gets slip-stacked, hence doubling the intensity that gets injected into Main Injector. Once in MI, the beam is accelerated to 120 GeV and sent to the NuMI (Neutrinos at the Main Injector) beam facility [8–10]. A description of the accelerator complex is shown in figure 3.1, including the experimental beamlines which feed neutrino, muon and fixed target experiments.

The work done for this thesis focuses on the Recycler Ring. The following chapter starts by giving a general description for the operation and physics of the Recycler Ring. The next sections introduce and motivate the compensation of third order resonances for high intensity operation.

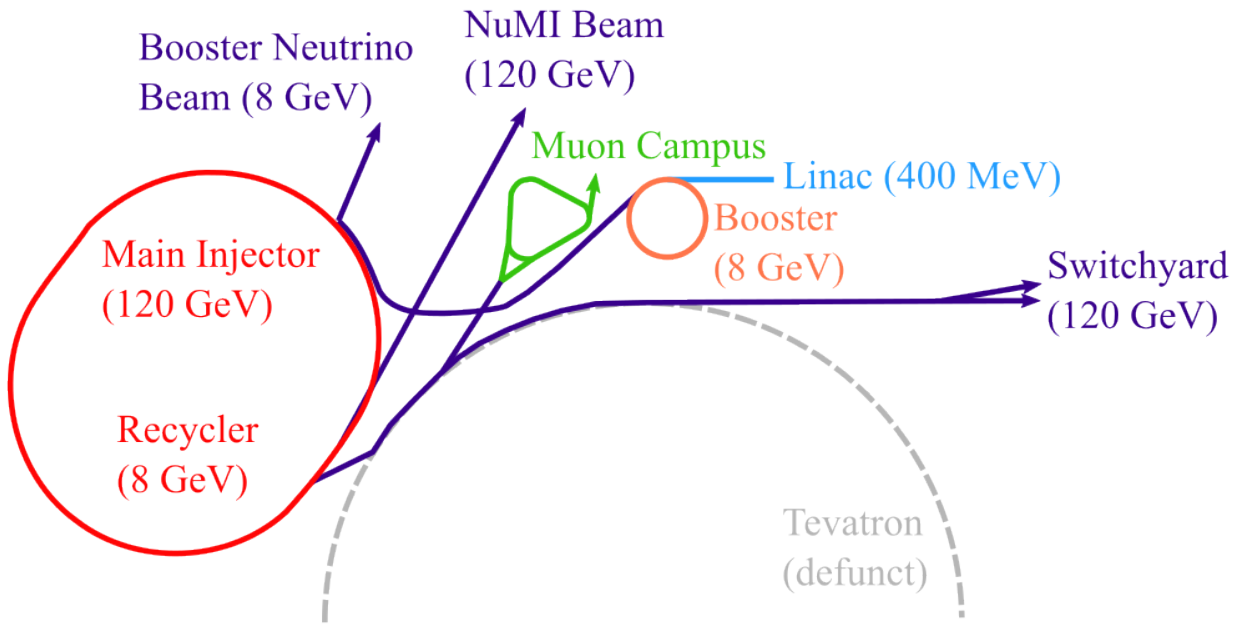


Figure 3.1 The past (Tevatron), present and future (PIP-II and LBNF) of the FNAL Accelerator Complex, taken from [3].

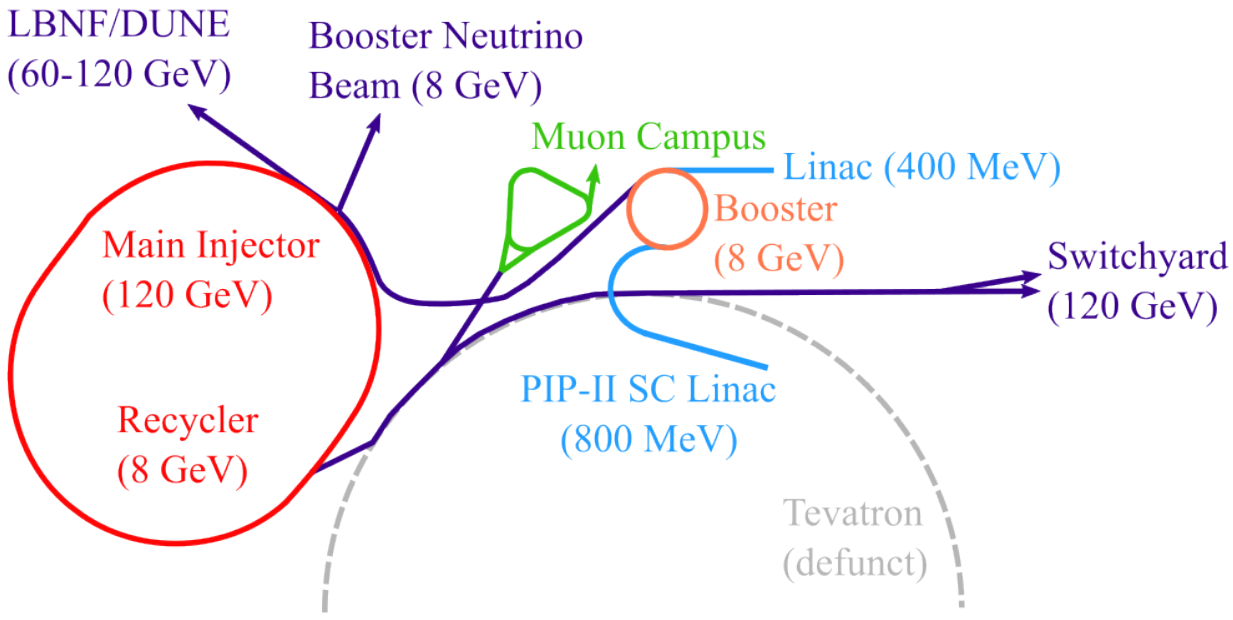


Figure 3.2 The past (Tevatron), present and future (PIP-II and LBNF) of the FNAL Accelerator Complex, taken from [3].

### 3.1 General Specifications

The RR is a permanent magnet storage ring operating at a fixed momentum of 8.835 Gev/c. [11] [12]

Table 3.1 Typical Recycler Ring properties for beam sent to NuMI

| **Parameter** | **Value** | **Unit** |
|---|---|---|
| Circumference | 3319 | m |
| Momentum | 8.835 | GeV/c |
| RF Frequency | 52.8 | MHz |
| RF Voltage | 80 | kV |
| Harmonic Number | 588 | |
| Synchrotron Tune | 0.0028 | |
| Slip Factor | $-8.6 \times 10^{-3}$ | |
| Superperiodicity | 2 | |
| Horizontal Tune | 25.43 | |
| Vertical Tune | 24.445 | |
| Horizontal Chromaticity | -6 | |
| Vertical Chromaticity | -7 | |
| 95% Normalized Emittance | 15 | $\pi$ mm mrad |
| 95% Longitudinal Emittance | 0.08 | eV s |
| Intensity | $5 \times 10^{10}$, $8 \times 10^{10}$ (PIP-II) | ppb |
| MI Ramp Time | 1.2, 1.133, 1.067 | s |
| Booster Frequency | 15, 20 (PIP-II) | Hz |

### 3.2 Tune Diagram and Resonances

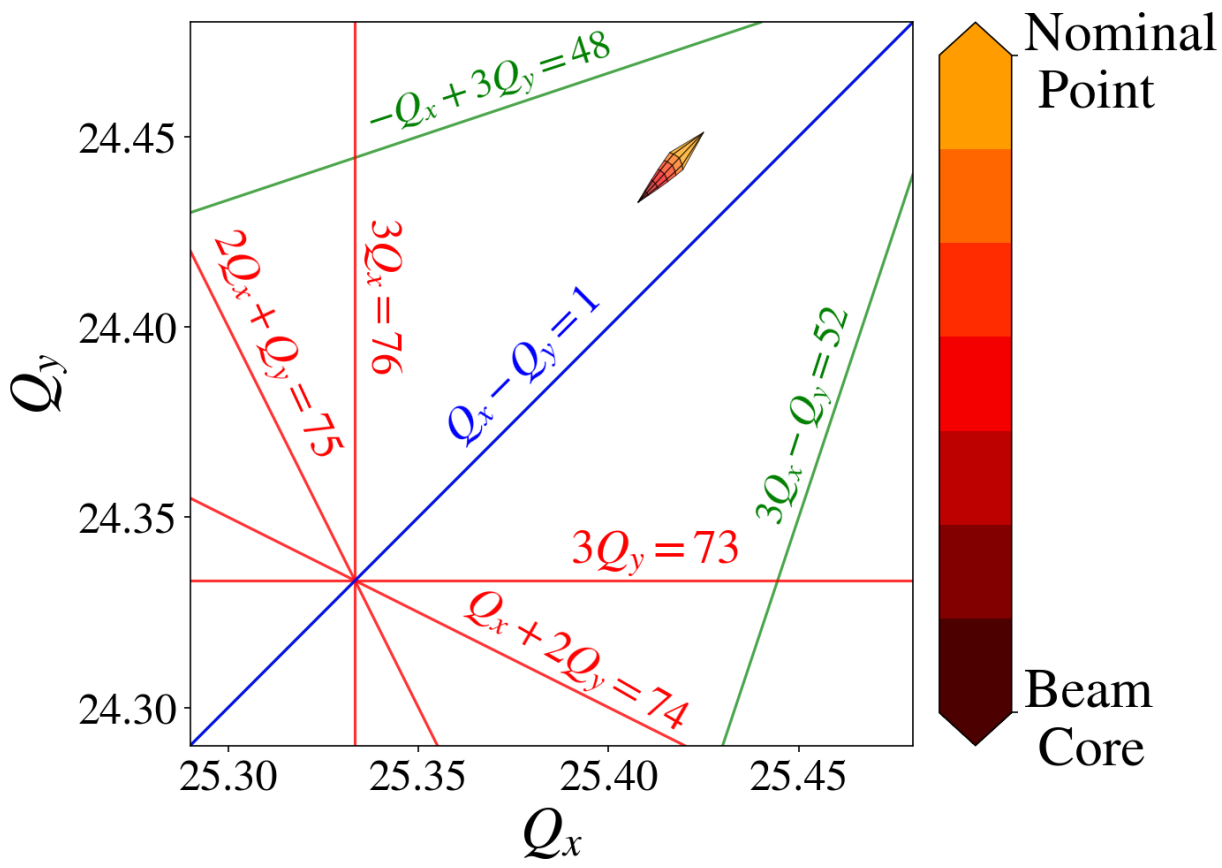


Figure 3.3 Approximate operational tune footprint at low intensities, i.e., 1e10 particles per bunch.

### 3.3 High Intensity and Tune Footprint

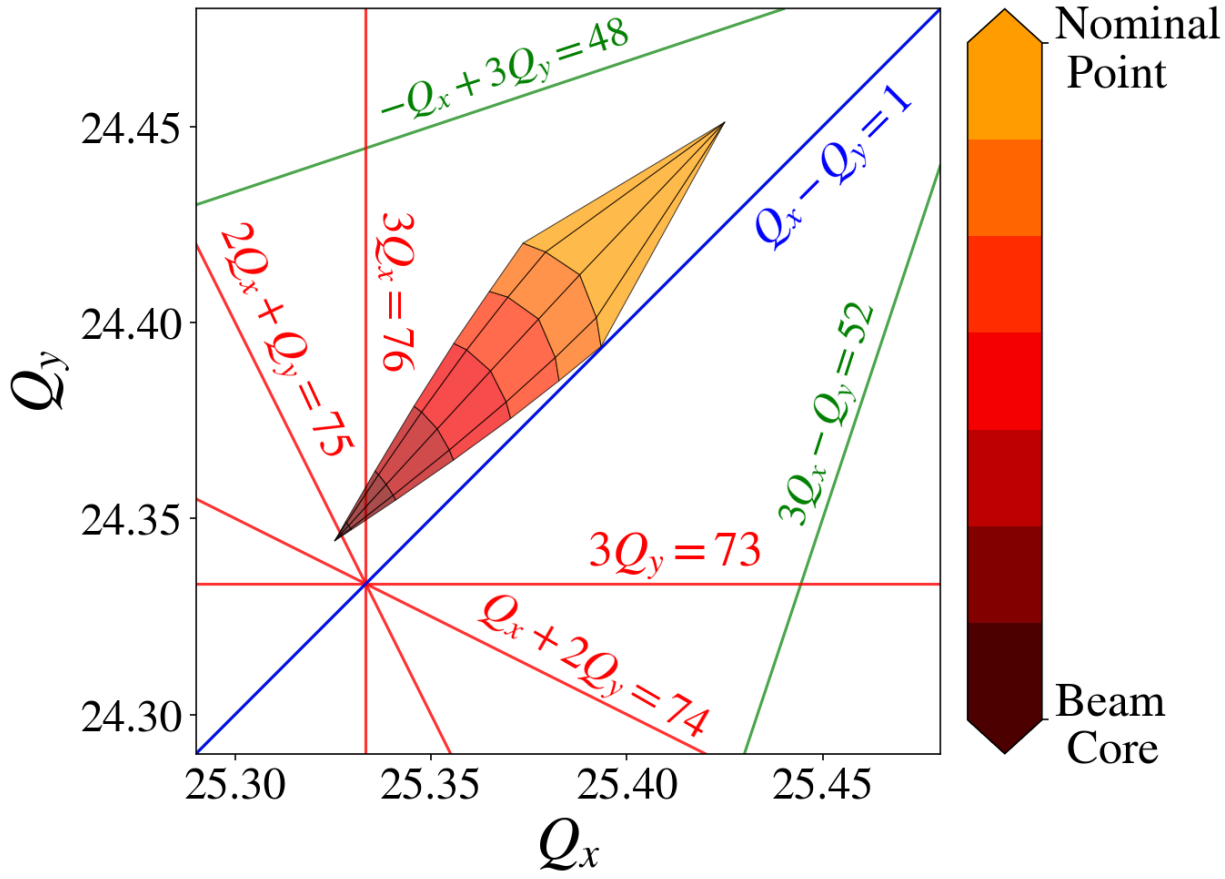


Figure 3.4 Approximate operational tune footprint at high intensities, i.e., 1e11 particles per bunch.

# CHAPTER 4

# COMPENSATION OF THIRD-ORDER RESONANCES AT LOW INTENSITIES

## 4.1 Global RDTs and Lattice Model

## 4.2 Measurement of Third Order RDTs

## 4.3 Compensation of RDTs

## 4.4 Optimization of Compensation Currents

## 4.5 Experimental Verification of Compensation

### 4.5.1 Dynamic Loss Map

### 4.5.2 Static Tune Scans

# CHAPTER 5

# RESONANCE COMPENSATION STUDIES AT THE CERN PROTON SYNCHROTRON BOOSTER

## 5.1 General specifications

## 5.2 Tune Diagram and Operation

## 5.3 Optimization Algorithms for Resonance Compensation

## 5.4 Experimental Verification of Compensation

# CHAPTER 6

# HIGH INTENSITY STUDIES

## 6.1 Global RDTs and Intensity-Dependent Effects

[13]

## 6.2 Space Charge Tune Shift

## 6.3 Measurement of Tune Shift

## 6.4 Static Tune Scans at Different Intensities

# CHAPTER 7

# CONCLUSIONS AND FUTURE WORK

[14] [15]

## BIBLIOGRAPHY


[1] Andrzej Wolski. *Beam Dynamics in High Energy Particle Accelerators*. 2nd. WORLD SCIENTIFIC, 2023. DOI: 10.1142/13333. eprint: https://www.worldscientific.com/doi/pdf/10.1142/13333. URL: https://www.worldscientific.com/doi/abs/10.1142/13333.

[2] T. Satogata. *Lecture Notes on Poisson Brackets and Lie Operators*. https://toddsatogata.net/2011-USPAS/lieAlgebras.pdf. Jan. 2008.

[3] P. Urschutz. "Measurement and Compensation of Betatron Resonances at the CERN PS Booster Synchrotron". PhD thesis. Vienna, Austria, 2004.

[4] R. Tomas Garcia. "Direct Measurement of Resonance Driving Terms in the Super Proton Synchrotron (SPS) of CERN using Beam Position Monitors". PhD thesis. Valencia, Spain, Jan. 2003.

[5] R Bartolini and F Schmidt. "Normal form via tracking or beam data". In: *Part. Accel.* 59 (1998), pp. 93–106. URL: https://cds.cern.ch/record/333077.

[6] Helmut Wiedemann. *Resonances*. Cham: Springer International Publishing, 2015, pp. 539–564. ISBN: 978-3-319-18317-6. DOI: 10.1007/978-3-319-18317-6_16. URL: https://doi.org/10.1007/978-3-319-18317-6_16.

[7] G. Jackson. *The Fermilab recycler ring technical design report. Revision 1.2*. Tech. rep. FNAL-TM-1991ON: DE97051388; BR: KAHEP. Fermilab, Nov. 1996. DOI: 10.2172/16029. URL: https://www.osti.gov/biblio/16029.

[8] S. Nagaitsev. *Fermilab Antiproton source, Recycler ring and Main Injector*. Tech. rep. FERMILAB-FN-0957-AD. Fermilab, Mar. 2013. DOI: 10.2172/1127965. URL: https://www.osti.gov/biblio/1127965.

[9] R. Ainsworth et al. "High intensity operation using proton stacking in the Fermilab Recycler to deliver 700 kW of 120 GeV proton beam". In: *Phys. Rev. Accel. Beams* 23 (12 Dec. 2020), p. 121002. DOI: 10.1103/PhysRevAccelBeams.23.121002. URL: https://link.aps.org/doi/10.1103/PhysRevAccelBeams.23.121002.

[10] P. Adamson et al. "The NuMI neutrino beam". In: *Nuclear Instruments and Methods in Physics Research Section A: Accelerators, Spectrometers, Detectors and Associated Equipment* 806 (2016), pp. 279–306. ISSN: 0168-9002. DOI: https://doi.org/10.1016/j.nima.2015.08.063. URL: https://www.sciencedirect.com/science/article/pii/S016890021501027X.

[11] M. Ball et al. *The PIP-II Conceptual Design Report*. Tech. rep. FERMILAB-TM-2649-AD-APC1516858. Fermilab, Mar. 2017. DOI: 10.2172/1346823. URL: https://www.osti.

gov/biblio/1346823.

[12] R. Ainsworth et al. “High intensity space charge effects on slip stacked beam in the Fermilab Recycler”. In: *Phys. Rev. Accel. Beams* 22 (2 Feb. 2019), p. 020404. DOI: 10.1103/PhysRevAccelBeams.22.020404. URL: https://link.aps.org/doi/10.1103/PhysRevAccelBeams.22.020404.

[13] N. Chelidze, R. Ainsworth, and K.J. Hazelwood. “The Effect of the Main Injector Ramp on the Recycler”. In: *Proc. 5th Int. Particle Accel. Conf. (NAPAC’22)* (Albuquerque, NM, USA). International Particle Accelerator Conference 5. JACoW Publishing, Geneva, Switzerland, Oct. 2022, MOPA19, pp. 90–92. ISBN: 978-3-95450-232-5. DOI: 10.18429/JACoW-NAPAC2022-MOPA19. URL: https://jacow.org/napac2022/papers/mopa19.pdf.

[14] C.E. Gonzalez-Ortiz, R. Ainsworth, and P.N. Ostroumov. “Third-Order Resonance Compensation at the FNAL Recycler Ring”. In: *Proc. IPAC’22* (Bangkok, Thailand). International Particle Accelerator Conference 13. JACoW Publishing, Geneva, Switzerland, July 2022, MOPOST050, pp. 195–198. ISBN: 978-3-95450-227-1. DOI: 10.18429/JACoW-IPAC2022-MOPOST050. URL: https://jacow.org/ipac2022/papers/mopost050.pdf.

[15] C.E. Gonzalez-Ortiz, R. Ainsworth, and P.N. Ostroumov. “Simultaneous Compensation of Third-Order Resonances at the FNAL Recycler Ring”. In: *Proc. IPAC’23* (Venezia). IPAC’23 - 14th International Particle Accelerator Conference 14. JACoW Publishing, Geneva, Switzerland, May 2023, pp. 3328–3331. ISBN: 978-3-95450-231-8. DOI: doi:10.18429/jacow-ipac2023-wepl112. URL: https://www.ipac23.org/preproc/pdf/WEPL112.pdf.

# APPENDIX

## YOUR APPENDIX